



NOVA

University of Newcastle Research Online

nova.newcastle.edu.au

Ruppert, Michael G.; Fairbairn, Matthew W.; Moheimani, S. O. Reza "Multi-mode resonant control of a microcantilever for atomic force microscopy", Published in Proceedings of the 2013 IEEE/ASME International Conference on Advanced Intelligent Mechatronics. (2013)

Available from: <http://dx.doi.org/10.1109/AIM.2013.6584071>

© 2013 IEEE. Personal use of this material is permitted. Permission from IEEE must be obtained for all other uses, in any current or future media, including reprinting/republishing this material for advertising or promotional purposes, creating new collective works, for resale or redistribution to servers or lists, or reuse of any copyrighted component of this work in other works.

Accessed from: <http://hdl.handle.net/1959.13/1295337>

Multi-Mode Resonant Control of a Microcantilever for Atomic Force Microscopy

Michael G. Ruppert¹, Matthew W. Fairbairn¹ and S.O. Reza Moheimani¹

Abstract—When operating the Atomic Force Microscope in tapping mode it is possible to decrease the quality factor of the microcantilever to enhance scan speed. A new field of Atomic Force Microscopy is evolving, which makes use of multiple frequency excitation and detection of the cantilever modes making it necessary to be able to control these modes and their response to excitation. This work proposes a multi-mode Q control approach utilizing positive position feedback, offering full control over the first two flexural modes of the cantilever. By completely damping the first mode and adjusting the quality factor of the second mode, it is possible to scan and obtain images at the second resonance frequency which improves image quality at high scan speeds due to the increased bandwidth of the z-axis feedback loop.

I. INTRODUCTION

The Atomic Force Microscope (AFM) [1] is a versatile instrument which is capable of producing high-resolution images on the nanometer scale. Imaging applications include, but are not limited to, images of inorganic material such as graphite [1] and silicon [2], and biological material such as DNA [3] or antibodies [4]. Images of samples are obtained by measuring the force between a sharp probe tip attached to a microcantilever and the surface of the sample. When operating in contact mode, the cantilever is dragged over the sample and is deflected in proportion to the height of surface structures. While a feedback controller is employed to maintain a constant cantilever deflection by positioning the piezoelectric scanner in the vertical (z-axis), this method may damage soft samples and lead to wear and tear of the probe's tip when scanning hard surfaces [5].

Operating the AFM in a dynamic mode overcomes this problem by oscillating the cantilever close to its first flexural resonance frequency. In intermittent contact mode, the tip touches the surface only for a short period of time in each oscillation cycle avoiding lateral friction forces. The parameters of the cantilever's oscillation such as amplitude, frequency and phase are modulated when oscillating in the proximity of the surface and can be used as a feedback signal. In this setup, one distinguishes between Amplitude Modulation AFM (AM-AFM), also named tapping-mode AFM, and Frequency Modulation AFM (FM-AFM). The feedback controller aims to keep a constant oscillation amplitude of the cantilever in AM-AFM, whereas in FM-AFM the feedback controller maintains a constant frequency shift [6]. Either way, the output of the regulating controller is proportional

to changes in the surface topography and can therefore be used to obtain a three dimensional image of the surface.

With the introduction of Q control [7] to modify the cantilever quality (Q) factor for improved scanning performance, a new field of research has opened. See references [8] and [9] for theoretical derivations and numerical simulations regarding the effects of externally changing the cantilever resonance. By actively damping the cantilever Q factor, an increase in scan speed has been reported in references [10] and [11]. Active Q control may be performed by velocity feedback if a costly velocity sensor is available and can be fitted in the limited space or, since most AFM systems are equipped with a displacement sensor, velocity is estimated by time-delay of the displacement signal. A major drawback of the time-delay approach is a possible instability of higher order modes. This problem was overcome by utilizing a resonant controller that guarantees closed loop stability when used in a collocated sensor-actuator environment. A block diagram of the AFM operated in tapping mode is shown in Fig. 1 where the outer (z-axis) feedback loop regulates the oscillation amplitude and the inner (Q control) feedback loop regulates the cantilever Q factor. In [12] a resonant controller was used to lower the Q factor of the first resonant mode and it was successfully shown that reducing the Q factor of the first mode improves imaging quality at higher scan speeds. When trying to minimize the noise introduced by the optical measurement system, a new method termed piezoelectric shunt control was presented in [13] to effectively control the cantilever Q factor and obtain improvement in both scan speed and image quality.

Scan speed is mainly limited by the bandwidth of the z-axis feedback loop [14], which is in turn limited by the transient response of the cantilever. As will be discussed in Section II, the cantilever transient response can be minimized by decreasing the cantilever Q factor or by increasing the resonance frequency. While with position feedback [15] only a marginal increase in the resonance frequency can be obtained, an increase in imaging bandwidth has been reported in [16] through the use of smaller cantilevers with higher resonance frequencies. Furthermore, by scanning on an higher eigenmode of the cantilever a reduction of the transient response time can be achieved, provided that the preceding modes are damped sufficiently ensuring the higher mode is dominant.

In conventional dynamic mode AFM the cantilever is excited and its response measured at a single frequency usually at the first flexural eigenmode. However, the motion of the cantilever while interacting with the surface is highly

*This work was supported by the Baden-Württemberg Stiftung and the Australian Research Council

¹School of Electrical Engineering and Computer Science, The University of Newcastle, Callaghan, NSW 2308, Australia

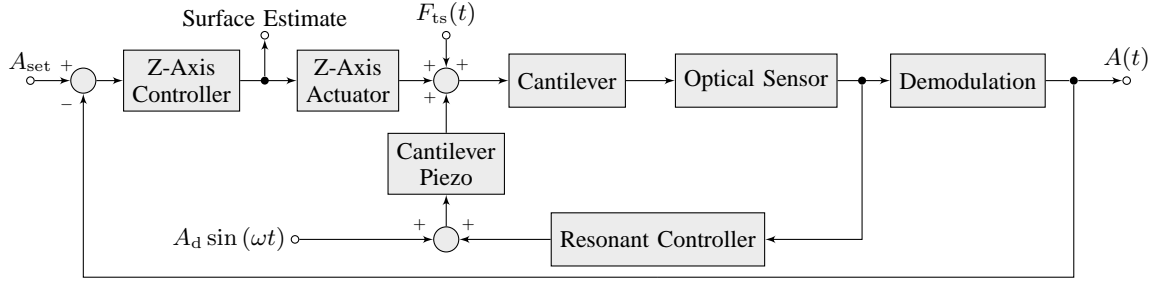


Fig. 1. Schematic setup of the AFM control loop. The outer feedback loop regulates the demodulated amplitude of the cantilever oscillation $A(t)$ to the setpoint amplitude A_{set} when the unknown tip-sample force $F_{ts}(t)$ is present, while the inner feedback loop regulates the cantilever Q factor.

nonlinear and information about the sample that is encoded in the deflection signal at frequencies other than the excitation frequency is lost during demodulation. To overcome this limitation in spatial resolution, another method of operation has emerged which makes use of vibration excitation and detection at several frequencies at once [17]. In bimodal AFM the cantilever is excited at its first two resonance frequencies simultaneously to acquire reciprocal information about the sample from each excited eigenmode. In [18] and [19] bimodal AM-AFM was successfully used to image graphite and isolated antibodies respectively.

This work introduces multi-mode Q control with guaranteed closed loop stability properties which can be employed in Multi-Frequency AFM. It is shown that the proposed control approach can be used to scan on the second flexural eigenmode of the cantilever which, due to the higher bandwidth, achieves higher scan speeds compared to scanning on the first flexural eigenmode. In Section II, the underlying analytical model is presented which justifies the motivation to lower the Q factor and increase the resonance frequency of the cantilever to increase scan speed. In Section III a multi-mode Q controller with guaranteed stability properties is presented and different controller design methods are shown. In Section IV a model of the cantilever is obtained via system identification and scans with the additional Q control feedback loop are conducted to show the effectiveness of the proposed control strategy.

II. CANTILEVER DYNAMICS

The microcantilever is a lightly damped flexible structure with n eigenmodes which can be described by a set of n decoupled second-order ordinary differential equations (ODE) [20]. Each ODE represents the motion of the structure $z_i(t)$ for a specific mode of vibration called the mode shape and is characterized in terms of the respective natural frequency $\omega_{0,i}$ and the quality factor Q_i . When driven by a sinusoidal signal with amplitude A_d and angular frequency ω , the equation of motion becomes

$$\ddot{z}_i(t) + \frac{\omega_{0,i}}{Q_i} \dot{z}_i(t) + \omega_{0,i}^2 z_i(t) = A_d \sin(\omega t). \quad (1)$$

Given the linear nature of the above approximation, the solution of (1) for any sinusoidal driving force is again a superposition of sinusoidal oscillations and can be expressed

as a linear combination of a transient z_t and a steady-state solution z_s

$$z(t) = z_t(t) + z_s(t). \quad (2)$$

With the cantilever initially being at rest at $t = 0$ the amplitude will increase from zero to the free air amplitude A_0 after switching on the excitation force. At steady state the oscillation is determined by a constant amplitude, frequency and phase shift. Solving the homogeneous equation for $i = 1$ of (1) with zero right-hand side and considering the underdamped case ($Q > \frac{1}{2}$) leads to the transient solution

$$z_t(t) = e^{-\frac{\omega_0}{2Q}t} (A_t \sin(\omega_d t + \phi_t)), \quad (3)$$

with the damped natural frequency

$$\omega_d = \omega_0 \sqrt{1 - \frac{1}{2Q^2}} \quad (4)$$

and A_t and ϕ_t being the amplitude and phase shift of the transient oscillation, respectively. The particular solution can be expressed as

$$z_s(t) = A_0 \sin(\omega t + \phi), \quad (5)$$

with A_0 being the free-air amplitude, ω the excitation frequency and ϕ the phase shift. The transient solution exponentially decays with a time constant

$$\tau = \frac{2Q}{\omega_0} \quad (6)$$

that is proportional to the quality factor and inversely proportional to the resonance frequency. It is desirable to have a fast decaying transient response since the output of the controller only resembles the surface when the cantilever is oscillating in its steady state. From (6) it can be seen that this can be achieved by decreasing Q or increasing ω_0 .

In modeling a lightly damped mechanical structure with collocated force actuators and position sensors, one obtains a negative imaginary system [21].

Applying the Laplace transform to

$$\begin{aligned} \ddot{z}_i(t) + \frac{\omega_{0,i}}{Q_i} \dot{z}_i(t) + \omega_{0,i}^2 z_i(t) &= \beta_i u(t) \\ y(t) &= \beta_i z(t), \end{aligned} \quad (7)$$

and assuming zero initial conditions, the infinite series transfer function from the cantilever piezoelectric actuator voltage $V(s)$ to cantilever deflection $D(s)$

$$G(s) = \frac{V(s)}{D(s)} = \sum_{i=1}^{\infty} \frac{\beta_i}{s^2 + \frac{\omega_{0,i}}{Q_i}s + \omega_i^2} \quad (8)$$

can be obtained [22], where β_i is the gain, Q_i is the quality factor and ω_i is the resonance frequency of the i -th mode. For the above transfer function to satisfy the negative imaginary property, as stated in [21], it has to be stable and satisfy the following condition:

$$j[G(j\omega) - G^*(j\omega)] \geq 0 \quad \forall \omega > 0. \quad (9)$$

Moreover, a transfer function is said to be strictly negative imaginary if (9) holds with a strict inequality sign. With $\beta_i > 0$, $Q_i > 0$ and $\omega_i > 0$ it is straightforward to show that all poles of (8) lie in the open half of the complex plane and that

$$j[G(j\omega) - G^*(j\omega)] = \sum_{i=1}^{\infty} \frac{2\beta_i\omega_i\omega \frac{1}{Q_i}}{(\omega_i^2 - \omega^2)^2 + (\omega_i\omega \frac{1}{Q_i})^2} > 0 \quad (10)$$

holds, thus rendering the cantilever strictly negative imaginary.

III. MULTI-MODE Q CONTROL

A. Negative imaginary feedback control system

The negative imaginary lemma derived in [23] states that the positive feedback interconnection, as depicted in Fig. 2, of a strictly negative imaginary (SNI) plant and a negative imaginary (NI) controller is internally stable if and only if the DC-gain condition $G(0)K(0) < 1$ is satisfied.

B. Positive Position Feedback Controller

The positive position feedback controller (PPF) [24] is of the form

$$K_{\text{PPF}} = \sum_{i=1}^M \frac{\gamma_i}{s^2 + 2\zeta_{c,i}\omega_{c,i}s + \omega_{c,i}^2}, \quad (11)$$

with γ_i , ζ_c and ω_c being the tunable controller parameters. From its structure it can be verified immediately that it satisfies the same strictly negative imaginary property as the cantilever transfer function.

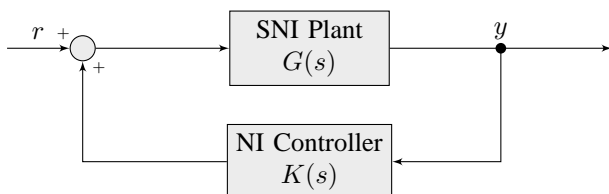


Fig. 2. Negative imaginary control system in positive feedback.

Another interesting property of the PPF controller can be derived as follows. Consider the first mode approximation of the plant when $i = 1$ in (1)

$$\ddot{z}(t) + \frac{\omega_0}{Q}\dot{z}(t) + \omega^2 z(t) = \beta u(t) \quad (12)$$

$$y(t) = \beta z(t) + Du(t) \quad (13)$$

with a non-zero feedthrough term D which is added to capture the effect of out-of-bandwidth modes [25] and the PPF controller

$$\ddot{x}(t) + 2\zeta_c\omega_c\dot{x}(t) + \omega_c^2 x(t) = \gamma y(t) \quad (14)$$

$$u(t) = \gamma x(t). \quad (15)$$

The closed loop system is obtained by substituting (15) in (12) and (13), (15) in (14)

$$\ddot{z}(t) + \frac{\omega_0}{Q}\dot{z}(t) + \omega^2 z(t) - \beta\gamma x(t) = 0 \quad (16)$$

$$\ddot{x}(t) + 2\zeta_c\omega_c\dot{x}(t) + (\omega_c^2 - \gamma D\gamma)x(t) - \gamma\beta z(t) = 0 \quad (17)$$

which yields

$$\begin{bmatrix} \ddot{z}(t) \\ \dot{x}(t) \end{bmatrix} + \underbrace{\begin{bmatrix} \frac{\omega_0}{Q} & 0 \\ 0 & 2\zeta_c\omega_c \end{bmatrix}}_{E=E^T} \begin{bmatrix} \dot{z}(t) \\ \dot{x}(t) \end{bmatrix} + \underbrace{\begin{bmatrix} \omega^2 & -\beta\gamma \\ -\gamma\beta & \omega_c^2 - \gamma D\gamma \end{bmatrix}}_{K=K^T} \begin{bmatrix} z(t) \\ x(t) \end{bmatrix} = 0. \quad (18)$$

For (18) to be stable, $E > 0$ and $K > 0$ must be satisfied. This holds true if

$$Q > 0, \omega > 0, \zeta_c > 0, \omega_c > 0 \quad (19)$$

$$\begin{bmatrix} \omega^2 & -\beta\gamma \\ -\gamma\beta & \omega_c^2 - \gamma D\gamma \end{bmatrix} > 0. \quad (20)$$

Rewriting (20)

$$\begin{bmatrix} \omega^2 & -\beta\gamma \\ -\gamma\beta & \omega_c^2 \end{bmatrix} - \begin{bmatrix} 0 \\ \gamma \end{bmatrix} D \begin{bmatrix} 0 & \gamma \end{bmatrix} > 0 \quad (21)$$

and applying the Schur-complement leads to

$$\begin{bmatrix} \omega^2 & -\beta\gamma & 0 \\ -\gamma\beta & \omega_c^2 & \gamma \\ 0 & \gamma & D^{-1} \end{bmatrix} > 0, \quad (22)$$

which is a linear matrix inequality (LMI) in the variables γ and ω_c^2 . Together with $\zeta_c > 0$ from (19), the set of stable PPF controllers is convex [22] which can be used for the controller design to ensure closed loop stability, as well as to calculate a feasible set of the controller parameters to initialize the optimization procedure.

C. Controller Design

The controller can be independently designed for the first and second eigenmode of the cantilever when i is set to the respective structure in (8) and (11). To achieve maximum

damping of the first mode, the controller design is formulated as an optimization problem of the form

$$\begin{aligned} \min_{\gamma, \zeta_c, \omega_c} \quad & \|G_{cl}(j\omega)\|_{\infty} \\ \text{s.t.} \quad & 0 \leq \gamma \leq \gamma_{\max} \\ & 0 \leq \zeta_c \leq \zeta_{c,\max} \\ & 0 \leq \omega_c \leq \omega_{c,\max} \\ & \begin{bmatrix} \omega^2 & -\beta\gamma & 0 \\ -\gamma\beta & \omega_c^2 & \gamma \\ 0 & \gamma & D^{-1} \end{bmatrix} > 0, \end{aligned} \quad (23)$$

with the cost function being the H_{∞} norm of the SISO linear system, which corresponds to the peak gain of the frequency response

$$\|G_{cl}(j\omega)\|_{\infty} = \max_{\omega} |G_{cl}(j\omega)| \quad (24)$$

and constraints γ_{\max} , $\zeta_{c,\max}$ and $\omega_{c,\max}$ corresponding to restrictions on the implementation. Simulation results of this procedure are shown in Fig. 3, in which it is seen that the open loop poles are shifted deeper in the left half of the complex plane, causing a damped frequency response. It can also be seen that at resonance two peaks have appeared, which is disadvantageous when performing scans at this specific frequency.

Therefore, to design a controller for the second eigenmode, a different approach has been taken which exactly places the real part of the closed loop poles $\Re(p_{i,cl})$ at a desired location $p_{i,des}$ by finding a solution to the optimization problem of

the form

$$\begin{aligned} \min_{\gamma, \zeta_c, \omega_c} \quad & J(\gamma, \zeta_c, \omega_c) \\ \text{s.t.} \quad & 0 \leq \gamma \leq \gamma_{\max} \\ & 0 \leq \zeta_c \leq \zeta_{c,\max} \\ & 0 \leq \omega_c \leq \omega_{c,\max} \\ & \begin{bmatrix} \omega^2 & -\beta\gamma & 0 \\ -\gamma\beta & \omega_c^2 & \gamma \\ 0 & \gamma & D^{-1} \end{bmatrix} > 0, \end{aligned} \quad (25)$$

with the cost function

$$\begin{aligned} J(\gamma, \zeta_c, \omega_c) = & \sum_{i=1}^4 (p_{i,des} - \Re(p_{i,cl}))^2 \\ & + \sum_{i=3}^4 |p_{i,cl} - p_{i-2,cl}|^2 \end{aligned} \quad (26)$$

that penalizes the difference between desired and actual pole locations and between poles that correspond to the same open loop poles if the closed loop poles are ordered in descending order. This way, it is ensured that the resonance peak will have a defined shape which is suitable for scanning. The desired real part of the closed loop poles can be found by setting a desired effective Q factor Q^* with the approximation

$$\Re(p_{1,2}) = \frac{\omega_2}{-2Q^*}, \quad (27)$$

which holds true for a second order system. A simulated example is shown in Fig. 4 in which it can be seen that the closed loop poles now do not separate resulting in an adequately shaped resonance peak, suitable for scanning.

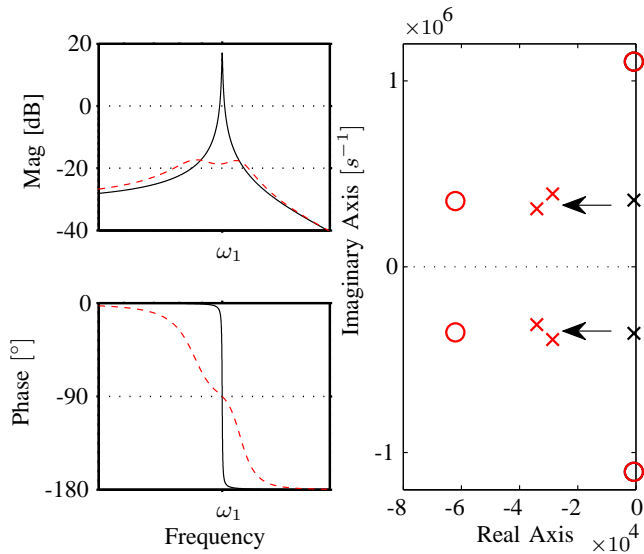


Fig. 3. Left: Open loop of first mode approximation (—) and closed loop with H_{∞} norm minimization PPF controller (---). Right: Open loop pole location (x) and closed loop pole location (x).

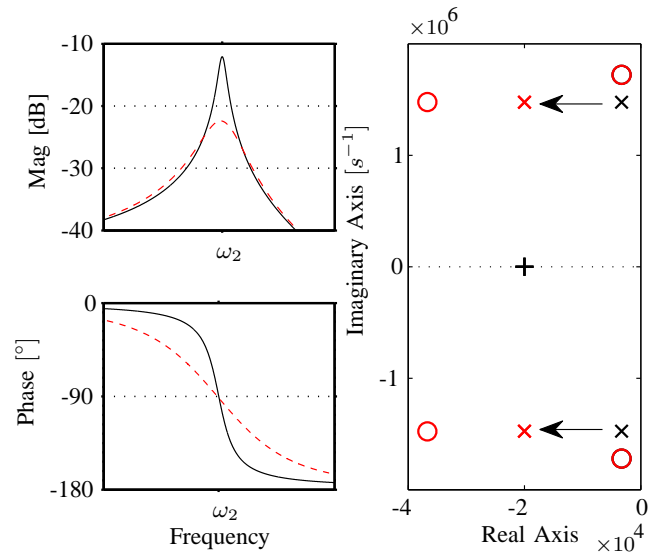


Fig. 4. Left: Open loop of second mode approximation (—) and closed loop with pole optimization PPF controller (---). Right: Desired pole location (+), open loop pole location (x) and closed loop pole location (x).

D. Properties

The frequency response of the multi-mode PPF controller to completely damp the first eigenmode and suitably lower the Q factor of the second eigenmode of the form

$$K(s) = \sum_{i=1}^2 \frac{\gamma_i}{s^2 + 2\zeta_{c,i}\omega_{c,i}s + \omega_{c,i}^2} \quad (28)$$

is shown in Fig. 5. It can be seen that the control energy is focused around the resonance peaks and furthermore the controller gain rolls off towards higher frequencies, benefiting the non-excitation of higher-order modes. At the resonance frequencies the phase crosses -90° , which resembles velocity feedback at that frequency resulting in a reduction of the Q factor. Furthermore, it can be observed that the phase stays within the bounds 0° to -180° which is a property of negative imaginary systems.

IV. EXPERIMENTAL RESULTS

A. System Identification

The AFM cantilever used in this work is the Dimension Micro-Actuated Silicon Probe (DMASP), a piezoelectric self actuated microcantilever manufactured by Bruker [26]. Frequency response data was obtained using a Polytec Micro System Analyzer (MSA-400) which provides data with a good signal-to-noise ratio over the desired bandwidth of 500 kHz. A sixth order state space model was obtained by means of a frequency domain subspace identification method [27]. From the model, the fixed structure form (8) for $n = 3$ is calculated with parameters shown in Table I. The fixed structure model along with the measured data is shown in Fig. 6. It can be observed that the frequency response displays the characteristic pattern of alternating poles and zeros, as it is typical for a negative imaginary system.

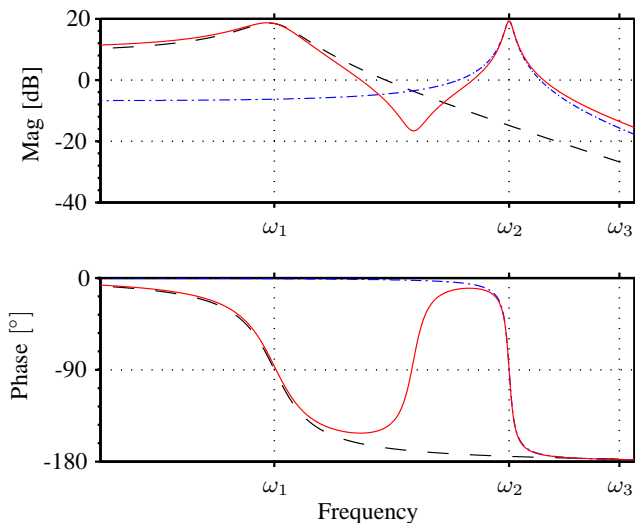


Fig. 5. PPF controller for first eigenmode (—), PPF controller for second eigenmode (---) and multi-mode Q controller (—).

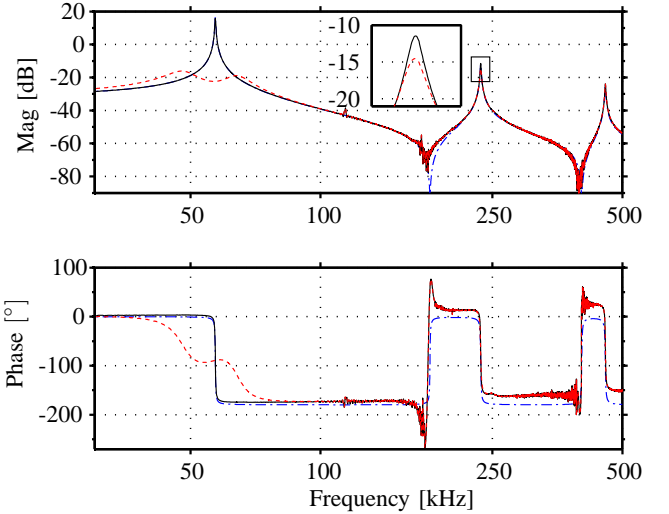


Fig. 6. Measured open loop frequency response (—), fixed structure model (---) and measured closed loop frequency response with multi-mode Q control (—).

B. Scanning on the Second Eigenmode

The proposed controller was implemented on a Field-Programmable Analog Array (FPAA). The Anadigm AN221E04 FPAA [28] offers sufficient bandwidth and provides enough flexibility through configurable analog modules (CAMS). The controller parameters were chosen to damp the first resonance frequency by an amount of approximately 25 dB to ensure that the second mode is the dominant mode and the Q factor of the second mode was set to $Q^* \approx 140$ (see Fig. 6). Scan experiments with an NT-MDT NTEGRA AFM [29] on a NT-MDT TGZ1 scan grating [29] with periodic features with step heights of $h = 21.6 \pm 1.5$ nm were conducted on the first eigenmode without Q control and on the second eigenmode with the proposed multi-mode Q controller. The images shown in Fig. 7 clearly show an improved image quality when scanning an area of $10 \mu\text{m} \times 10 \mu\text{m}$ at a speed of $156.3 \mu\text{m/s}$. The cross-section analysis of both scans shown in Fig. 8 demonstrates how the scan on the second eigenmode with multi-mode Q control tracks the features of the sample more accurately.

V. CONCLUSIONS

This work has introduced multi-mode Q control with positive position feedback for a microcantilever to be used in tap-

TABLE I
PARAMETERS OF THE FIXED STRUCTURE MODEL.

Mode	Mode shape	f_i [kHz]	Q_i	β_i
1		57.07	268	$8.69 \cdot 10^4$
2		234.92	234	$6.10 \cdot 10^4$
3		456.67	233	$5.10 \cdot 10^4$

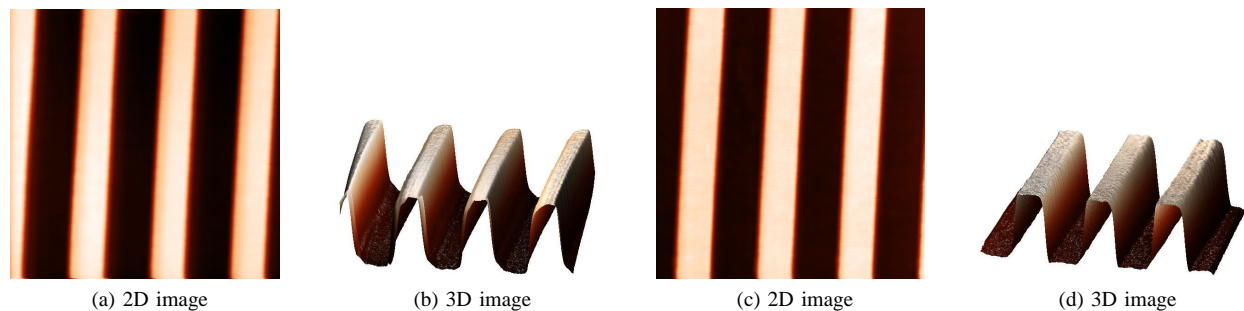


Fig. 7. (a) and (b): Scan on the first eigenmode at $156.3\mu\text{m/s}$ without Q control. (c) and (d): Scan on the second eigenmode at $156.3\mu\text{m/s}$ with multi-mode Q control.

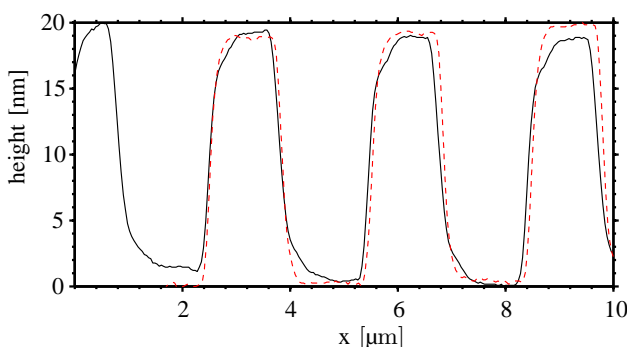


Fig. 8. Cross section analysis of image obtained on first eigenmode without Q control (—) and of image obtained on second eigenmode with multi-mode Q control (---).

ping mode AFM. Scans obtained on the second eigenmode of the cantilever, using the proposed controller, produced higher quality images at higher scan speeds than without Q control on the first eigenmode. In subsequent work, the authors aim to use multi-mode Q control within the context of Multi-Frequency AFM.

REFERENCES

- [1] G. Binnig, C. Gerber, E. Stoll, T. R. Albrecht, and C. F. Quate, "Atomic resolution with atomic force microscope," *Europhysics Letters*, vol. 3(12), pp. 1281–1286, 1987.
- [2] F. J. Giessibl, "Atomic resolution of the silicon (111)-(7x7) surface by atomic force microscopy," *Science*, vol. 267, pp. 68–71, 1995.
- [3] D. Anselmetti, R. Lthi, E. Meyer, R. Richmond, M. Dreier, and H. J. Frommer, J. E. Gntherodt, "Imaging of biological materials with dynamic force microscopy," *Nanotechnology*, vol. 5, pp. 87–94, 1994.
- [4] A. San Paulo and R. Garcia, "High-resolution imaging of antibodies by tapping-mode atomic force microscopy: attractive and repulsive tip-sample interaction regimes," *Biophysical Journal*, vol. 78(3), pp. 1599–1605, 2000.
- [5] B. Bhushan, *Springer Handbook of Nanotechnology*. Springer-Verlag Berlin Heidelberg, 2010.
- [6] R. Garcia and R. Perez, "Dynamic atomic force microscopy methods," Instituto de Microelectronica de Madrid, CSIC, Tech. Rep., 2002.
- [7] J. Mertz, O. Marti, and J. Mlynek, "Regulation of a microcantilever response by force feedback," *Applied Physics Letters*, vol. 62, pp. 2344–2346, 1993.
- [8] T. R. Rodriguez and R. Garcia, "Theory of Q control in atomic force microscopy," *Applied Physics Letters*, vol. 82, no. 26, p. 084311, 2003.
- [9] H. Hölischer and U. D. Schwarz, "Theory of amplitude modulation atomic force microscopy with and without Q-control," *International Journal of Non-Linear Mechanics*, vol. 42, pp. 608–625, 2007.
- [10] T. Sulchek, R. Hsieh, J. D. Adams, G. G. Yaralioglu, S. C. Minne, and C. F. Quate, "High-speed tapping mode imaging with active Q control for atomic force microscopy," *Applied Physics Letters*, vol. 76(11), pp. 1473–1475, 2000.
- [11] T. Sulchek, G. G. Yaralioglu, and C. F. Quate, "Characterization and optimization of scan speed for tapping-mode atomic force microscopy," *Review of Scientific Instruments*, vol. 73(8), pp. 2928–2936, 2002.
- [12] M. Fairbairn and S. O. R. Moheimani, "Resonant control of an atomic force microscope micro-cantilever for active Q-control," July 2012, accepted for publication.
- [13] M. Fairbairn, S. O. R. Moheimani, and A. J. Fleming, "Q control of an atomic force microscope micro-cantilever: A sensorless approach," *Journal of Microelectromechanical Systems*, vol. 20, no. 6, pp. 1372–1381, 2011.
- [14] M. Fairbairn, "Feedback control of the atomic force microscope micro-cantilever for improved imaging," Ph.D. dissertation, The University of Newcastle, 2013.
- [15] B. Orun, S. Necipoglu, C. Basdogan, and L. Guvenc, "State feedback control for adjusting the dynamic behavior of a piezoactuated bimorph atomic force microscopy probe," *Review of Scientific Instruments*, vol. 80, pp. 063 701–1–7, 2009.
- [16] D. A. Walters, J. P. Cleveland, N. H. Thomson, P. K. Hasma, M. A. Wendman, G. Gurley, and V. Elings, "Short cantilevers for atomic force microscopy," *Review of Scientific Instruments*, vol. 67, p. 3583, 1996.
- [17] R. Garcia and E. T. Herruzo, "The emergence of multifrequency force microscopy," *Nature Nanotechnology*, vol. 7, pp. 217–226, 2012.
- [18] R. Proksch, "Multifrequency, repulsive-mode amplitude-modulated atomic force microscopy," *Applied Physics Letters*, vol. 89, pp. 113–121, 2006.
- [19] N. F. Martinez, J. R. Lozano, E. T. Herruzo, F. Garcia, C. Richter, T. Sulzbach, and R. Garcia, "Bimodal atomic force microscopy imaging of isolated antibodies in air and liquids," *Nanotechnology*, vol. 19, p. 384011, 2008.
- [20] S. S. Rao, *Mechanical Vibrations*. Addison-Wesley Publishing Company, 1995.
- [21] I. R. Petersen and A. Lanzon, "Feedback control of negative imaginary systems," *IEEE Control Systems Magazine*, vol. 30, no. 5, pp. 54–72, 2010.
- [22] S. R. Moheimani and A. J. Fleming, *Piezoelectric Transducers for Vibration Control and Damping*. Springer-Verlag London, 2006.
- [23] A. Lanzon and I. R. Petersen, "Stability robustness of a feedback interconnection of systems with negative imaginary frequency response," *IEEE Transactions on Automatic Control*, vol. 53, pp. 1042–1046, 2008.
- [24] J. Fanson and T. K. Caughey, "Positive position feedback control for large space structures," *AIAA Journal*, vol. 28, pp. 717–724, 1990.
- [25] R. S. O. Moheimani, "Minimizing the effect of out of bandwidth modes in truncated structure models," *Journal of Dynamic Systems, Measurement and Control*, vol. 122, pp. 237–239, 2000.
- [26] Bruker, "Bruker afm probes catalog," Bruker, Tech. Rep., 2012.
- [27] T. McKelvey, "Subspace methods for frequency domain data," *Proceedings of the 2004 American Control Conference*, vol. 1, pp. 673–678, 2004.
- [28] Anadigm, "AN221E04 datasheet," Anadigm, Tech. Rep., 2010.
- [29] NT-MDT. (2013) [online]. Available: <http://www.ntmdt.com/>.